

F. Namouni · M. Guzzo

# The accelerated Kepler problem

Received: date / Accepted: date

**Abstract** The accelerated Kepler problem is obtained by adding a constant acceleration to the classical two-body Kepler problem. This setting models the dynamics of a jet-sustaining accretion disk and its content of forming planets as the disk loses linear momentum through the asymmetric jet-counterjet system it powers. The dynamics of the accelerated Kepler problem is analyzed using physical as well as parabolic coordinates. The latter naturally separate the problem's Hamiltonian into two unidimensional Hamiltonians. In particular, we identify the origin of the secular resonance in the accelerated Kepler problem and determine analytically the radius of stability boundary of initially circular orbits that are of particular interest to the problem of radial migration in binary systems as well as to the truncation of accretion disks through stellar jet acceleration.

**Keywords** Kepler problem · stellar jets · extrasolar planets · stellar binaries

## 1 Introduction

The recent studies of the consequences of the acceleration induced by stellar jets on extrasolar planets and protoplanetary disks (Namouni 2005, 2007,

---

F. Namouni  
Laboratoire Cassiopée, CNRS UMR 6202  
Observatoire de la Côte d'Azur, BP 4229, Nice 06304, France  
Tel.: +33-492-003023  
Fax: +33-492-003118  
E-mail: namouni@obs-nice.fr

M. Guzzo  
Dipartimento di Matematica Pura ed Applicata  
Università degli Studi di Padova, via Trieste 63, 35121 Padova, Italy  
Tel.: +39-049-8271416  
Fax: +33-049-8271204  
E-mail: guzzo@math.unipd.it

hereafter Papers I, II; Namouni and Zhou 2006) have shown that the basic dynamics of these systems rely on the accelerated Kepler problem (hereafter AKP). Although it is uncommon in celestial mechanics, the problem obtained by adding a constant acceleration to one of the two bodies in an  $r^{-1}$  potential is at the basis of the Stark effect in quantum mechanics (Brandsen and Joachain 1989). In this case, the acceleration models the constant electric field applied to an atom.

An interesting property of the AKP is its integrability. This result was obtained by Epstein (1916) who used the Hamilton-Jacobi approach in terms of parabolic coordinates to separate the AKP into two unidimensional Hamiltonians (Landau and Lifschitz 1969). The integrability of the AKP in the position-velocity space was expressed by Redmond (1964) who derived a generalized Runge-Lenz invariant for the Stark effect. This invariant together with the energy and the angular momentum component along the direction of acceleration are the three integrals of the AKP. Recently, it was recognized that some of the dynamical consequences of time-variable jet-induced acceleration on the evolution of accretion disks and the forming planets they contain can be ascertained from the AKP (i.e. from the dynamics associated with a time-independent acceleration). To this end, analytical derivations in terms of the physical variables (positions, velocities, orbital elements) as well as perturbation theory through secular averaging and sudden impulse methods were used to determine the eccentricity and inclination excitation of extrasolar planets (Paper I) as well as the vertical profile of jet-sustaining accretion disks (Paper II).

The use of parabolic coordinates has the advantage of reducing the AKP into two integrable unidimensional problems. This however comes at a price: parabolic coordinates are not physical. Consequently, the aim of this paper is to link the two analytical approaches of perturbation theory and parabolic coordinates in order to give a canonical interpretation of the physical properties described in the works mentioned above.

The paper is organized as follows: in Section 2, we show how the AKP arises in Keplerian systems with asymmetric momentum loss. In Section 3, we compare some of the AKP's simple qualitative features to those of the classical Kepler problem. Section 4 is devoted to the AKP's formulation in parabolic coordinates. The secular resonance at the basis of the eccentricity excitation of extrasolar planets is studied in section 5 and its origin in the non-averaged problem is given in terms of parabolic coordinates. In section 6, we derive the dependence of the Keplerian boundary radius on the initial inclination for circular orbits. Section 7 contains further directions of research in the AKP.

## 2 From the classical Kepler problem to the AKP

Consider a two-body Kepler problem where the larger mass object is losing linear momentum at the constant rate  $\dot{\mathbf{P}}_{\text{loss}}$ . The equations of motion of the

two bodies in an inertial frame are given as:

$$m \frac{d\mathbf{v}}{dt} = -\frac{GM(\mathbf{x} - \mathbf{X})}{|\mathbf{x} - \mathbf{X}|^3}, \quad M \frac{d\mathbf{V}}{dt} = \frac{Gm(\mathbf{x} - \mathbf{X})}{|\mathbf{x} - \mathbf{X}|^3} + \dot{\mathbf{P}}_{\text{loss}}, \quad (1)$$

where  $m$ ,  $M$ ,  $\mathbf{x}$ ,  $\mathbf{X}$ ,  $\mathbf{v}$ ,  $\mathbf{V}$  are the masses, positions and velocities of the two bodies and  $G$  is the gravitational constant. In terms of the center of mass and relative motion coordinates,  $\mathbf{x}_r = \mathbf{x} - \mathbf{X}$ ,  $(m + M)\mathbf{x}_g = m\mathbf{x} + M\mathbf{X}$  and the corresponding velocities,  $\mathbf{v}_r$ ,  $\mathbf{v}_g$ , the equations of motion are written as:

$$\frac{d\mathbf{v}_g}{dt} = \frac{\dot{\mathbf{P}}_{\text{loss}}}{(m + M)}, \quad \frac{d\mathbf{v}_r}{dt} = -\frac{G(m + M)}{|\mathbf{x}_r|^3} \mathbf{x}_r - \frac{\dot{\mathbf{P}}_{\text{loss}}}{M}. \quad (2)$$

These equations show that the motion of the center of mass is accelerated in the inertial frame by an amount equal to the ratio of the momentum loss rate to the total mass of the system. The relative motion of the small body remains independent of the center of mass's motion while it is accelerated in the opposite direction to momentum loss by the ratio of the momentum loss rate to the central mass.

Calling  $\mathbf{A} = -\dot{\mathbf{P}}_{\text{loss}}/M$  the constant acceleration of the relative motion and dropping the index  $r$  for simplicity, the relative motion of the smaller object around the larger one is given by:

$$\frac{d\mathbf{v}}{dt} = -\frac{k}{|\mathbf{x}|^3} \mathbf{x} + \mathbf{A}, \quad (3)$$

where  $k = G(M + m)$ . This equation defines the accelerated Kepler problem. It describes the dynamical evolution of a planet embedded in a jet-sustaining disk that loses mass and linear momentum from its inner parts (the so-called jet launching region, Paper II).

### 3 Constants of motion and equilibrium points

As the perturbing acceleration is constant, the dynamical problem described by (3) remains conservative and amounts to the addition of the potential  $R = \mathbf{A} \cdot \mathbf{x}$  to the two-body Kepler problem. This in turn gives the energy integral of the AKP as:

$$E = \frac{v^2}{2} - \frac{k}{|\mathbf{x}|} - \mathbf{A} \cdot \mathbf{x}. \quad (4)$$

The acceleration  $\mathbf{A}$  defines a preferred direction in the AKP. As a result, the projection of the specific angular momentum  $\mathbf{h} = \mathbf{x} \times \mathbf{v}$  along this direction,

$$h_z = \mathbf{h} \cdot \mathbf{A}/A, \quad (5)$$

is conserved as  $\dot{\mathbf{h}} = \mathbf{x} \times \mathbf{A}$ . The third integral (Redmond 1964) is given as:

$$\beta = k \frac{\mathbf{A} \cdot \mathbf{e}}{A} + \frac{(\mathbf{x} \times \mathbf{A})^2}{2A}, \quad (6)$$

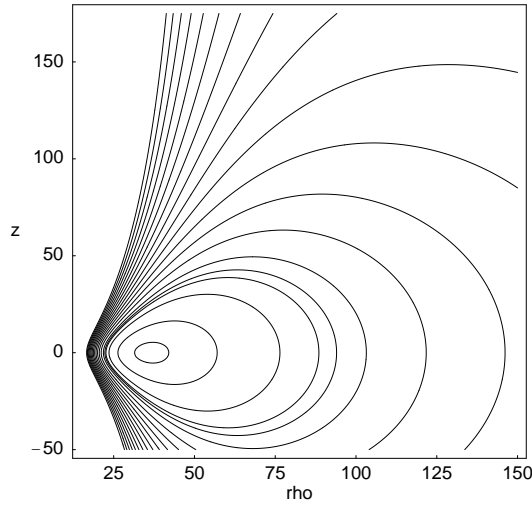


**Fig. 1** Zero-velocity curves of the classical Kepler problem in the cylindrical coordinate plane  $(\rho, z)$ . The unit distance is the Astronomical Unit (AU). The central object's mass is equal to the Sun's and the value of  $h_z$  used in the expression of  $W$  is that of a planar circular orbit at  $\rho = 36$  AU.

where  $\mathbf{e} = \mathbf{v} \times \mathbf{h}/k - \mathbf{x}/|\mathbf{x}|$  is the Runge-Lenz vector. The constant  $\beta$  replaces the Runge-Lenz vector of the classical Kepler problem.

To further compare the AKP with the classical Kepler problem, we examine its orbits of least energy. As the acceleration imposes a preferred direction, we choose a reference frame where the  $z$ -axis is directed along  $\mathbf{A}$ . Using the conservation of  $h_z$ , the energy integral (4) can be written as:

$$E = \frac{\dot{\rho}^2 + \dot{z}^2}{2} + W(\rho, z), \quad \text{where } W(\rho, z) = \frac{h_z^2}{2\rho^2} - \frac{k}{\sqrt{\rho^2 + z^2}} - Az, \quad (7)$$

and where  $\rho$  and  $z$  are the usual cylindrical coordinates in the plane orthogonal to  $\mathbf{A}$ . For a given value of  $h_z$ , the zero-velocity curves (level curves of  $W$ ) are shown in Fig. 1 for the classical Kepler problem and in Fig. 2 for the AKP. For the classical Kepler problem, only a stable equilibrium associated with circular motion is present. In the case of the AKP, the addition of the acceleration potential and its odd-symmetry introduce a new unstable equilibrium as well as a motion separatrix. The two equilibrium orbits (stable and unstable) of the AKP are located above the reference plane,  $z = 0$ , that contains the central object. The separatrix denotes the boundary where the acceleration from the central object matches the amplitude of the perturbing acceleration. Motion outside the separatrix is unbounded. To determine the location of the equilibrium points, we minimize the energy integral with respect to  $\dot{\rho}$ ,  $\dot{z}$ ,  $\rho$ , and  $z$ . The first two derivatives yield  $\dot{\rho} = \dot{z} = 0$  showing that least energy orbits are circular and planar. The derivative with respect to  $\rho$  yields the orbital rotation rate as a function of the projection of the

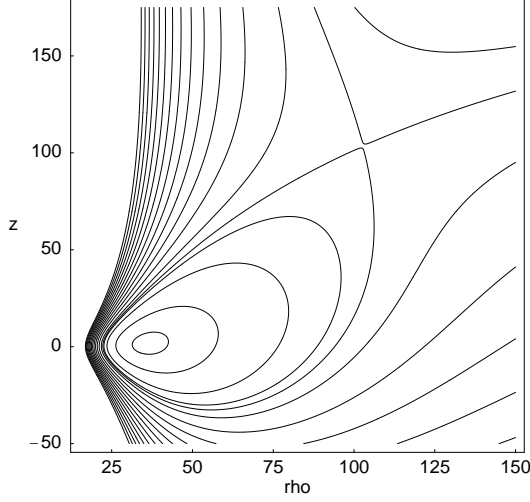


**Fig. 2** Zero-velocity curves of the AKP in the cylindrical coordinate plane  $(\rho, z)$ . The unit distance is the Astronomical Unit (AU). A constant vertical acceleration of amplitude  $A = 2 \times 10^{-10} \text{ km s}^{-2}$  was added to the classical Kepler problem of Fig. 1. The odd-symmetry of the acceleration's potential removes the reflection symmetry of the Kepler problem with respect to  $z$ . The region of bounded motion is restricted by the appearance of the unstable orbit at  $(\rho, z) = (102.8, 103.5)$ .

angular momentum on the direction of acceleration,  $h_z$ . Using the fact that orbits are planar and circular,  $h_z = n\rho^2$  and the orbital rotation rate:

$$n = \left[ \frac{k}{(\rho^2 + z^2)^{3/2}} \right]^{\frac{1}{2}}. \quad (8)$$

The derivative with respect to  $z$  amounts to equating the vertical acceleration,  $\mathbf{A}$ , and the vertical pull of the central object and yields

$$\rho = \left[ \left( \frac{kz}{A} \right)^{\frac{2}{3}} - z^2 \right]^{\frac{1}{2}}. \quad (9)$$

The circular orbits hover above the central object increasingly higher with distance. In other words, a circular orbit in the AKP is still planar but the corresponding orbital plane no longer contains the central object. The latter becomes increasingly distant from that plane as the orbital radius increases. Figure (3) shows the family of circular orbits of the AKP in the  $\rho z$ -plane. The uppermost orbit is located at  $\rho = 0$  and  $z = \sqrt{k/A}$ .

The locus of least energy orbits given by equations (8) and (9) does not indicate where the stable orbits end and the unstable orbits start. To find this limit, we express the specific angular momentum,  $h_z$ , for the least energy orbits (9) as a function of  $z$ . As the equilibria of  $W$  in the  $\rho z$ -plane are determined by the same  $h_z$ , their coordinates are found by solving for  $z$  at

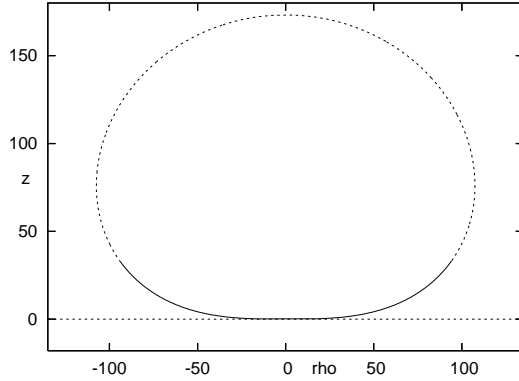


**Fig. 3** Least energy orbits of the AKP in the  $\rho z$ -plane. The system's parameters are those of Fig. 2. The solid line stands for the stable equilibrium orbits (the sombreiro profile) and the dashed line for the unstable equilibrium orbits (see Fig. 4 for more details).

constant  $h_z$  and using equation (9) to determine  $\rho$ . The maximum of  $h_z(z)$  is reached at:

$$z_{\text{crit}} = \left[ \frac{k}{27A} \right]^{\frac{1}{2}} \quad \text{and} \quad \rho_{\text{crit}} = \left[ \frac{8k}{27A} \right]^{\frac{1}{2}}. \quad (10)$$

This location determines the last stable planar circular orbit of the AKP. Figure (4) shows the function  $h_z^2(z)$  as well as  $\rho(z)$  (9). The maximum of  $h_z$  is where the stable and unstable points meet; above this value of  $h_z$  motion is unbounded in all space. For  $z < z_{\text{crit}}$ , planar circular orbits are stable and their profile in the  $\rho z$ -plane has the shape of a sombreiro curved along the direction of acceleration (Fig. 3). In Paper II, the sombreiro profile was identified as the instantaneous state of least energy of a jet-sustaining disk. This profile was used to ascertain the changes in the temperature, hydrostatic equilibrium and heating of the disk.

Lastly, we remark that the existence of the constant of motion  $\beta$  shows that the separatrix of  $W$  is pendulum-like and does not involve any kind of chaotic motion. Orbits that are set up near the unstable point such as that in Figures 7 and 8 of Paper I tend to escape after a long time (relative to the orbital period) only because of the discrete nature of the numerical scheme used to integrate the orbit. In section 6, we discuss further the outer boundary of initially circular orbits whose orbital plane is inclined to the direction of acceleration such as those studied in Paper I. Before doing so, we first introduce the formulation of the AKP in parabolic coordinates that will be needed in sections 5 and 6.

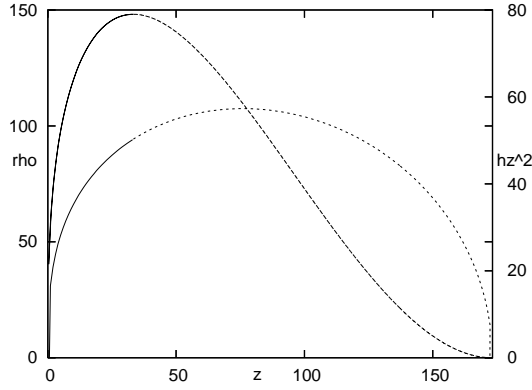


**Fig. 4** The identification of the equilibrium orbits' stability through the vertical component of angular momentum. The system's parameters are those of Fig. 3. Least energy orbits (lower maximum curve) are shown in the  $z\rho$ -plane (left scale). The function  $h_z^2(z)$  (higher maximum curve, right scale) is determined from the equilibrium orbits (Eqns. 8 and 9) and normalized to the angular momentum of a circular orbit at 1 AU. The function  $h_z^2(z)$  yields two values of  $z$  for a given value of  $h_z$ . These are the stable (solid line) and unstable (dashed line) equilibria of Fig. 2. The maximum of  $h_z^2(z)$  denotes the outer edge of the sombrero profile.

#### 4 The AKP in parabolic coordinates

Parabolic coordinates  $(\xi, \eta, \theta)$  are related to the cylindrical coordinates  $(\rho, z, \theta)$  through (Landau and Lifschitz 1969):

$$z = \frac{1}{2}(\xi - \eta), \quad \rho = \sqrt{\xi\eta}. \quad (11)$$

In terms of the orbital radius  $r^2 = \rho^2 + z^2$ , these coordinates are written as:

$$\xi = r + z, \quad \eta = r - z. \quad (12)$$

The conjugate momenta of parabolic coordinates are given by:

$$p_\xi = \frac{\dot{\xi}}{4\xi}(\xi + \eta), \quad p_\eta = \frac{\dot{\eta}}{4\eta}(\xi + \eta), \quad p_\theta = \xi\eta\dot{\theta}. \quad (13)$$

The Hamiltonian of the AKP can now be written in terms of the parabolic coordinates and momenta as:

$$H = 2 \frac{\xi p_\xi^2 + \eta p_\eta^2}{\xi + \eta} + \frac{p_\theta^2}{2\xi\eta} - \frac{2k}{\xi + \eta} - \frac{A}{2}(\xi - \eta), \quad (14)$$

where we used the relations (11) and (12) in the expressions of the gravitational potential as well as the acceleration potential  $R = Az$  (third and fourth terms on the right hand side). As the Hamiltonian is autonomous and independent of  $\theta$ , we recover the two constants of motion: the energy (4),

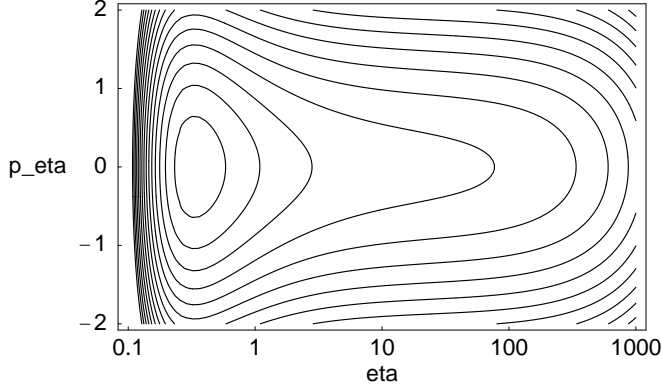


**Fig. 5** Contour plots of the Hamiltonian (16) in the  $\eta p_\eta$ -plane with the parameters  $h_z = 1$ ,  $A = 0.1$ ,  $\beta = 1$  and  $k = 2$ . Motion is always bounded.

$H = E$ , and the angular momentum component along the direction of acceleration (5),  $p_\theta = h_z$ . By applying the Hamilton-Jacobi approach with the separation of variables method, it can be shown (Epstein 1916, Landau and Lifschitz 1969) that the Hamiltonian (14) decouples into two unidimensional Hamiltonians that are related by the energy  $E$ , the vertical component of angular momentum,  $h_z$  and a third integral,  $\beta$  defined in equation (6), and given by:

$$\beta = 2\eta p_\eta^2 + \frac{h_z^2}{2\eta} + \frac{A\eta^2}{2} - E\eta - k, \quad -\beta = 2\xi p_\xi^2 + \frac{h_z^2}{2\xi} - \frac{A\xi^2}{2} - E\xi - k. \quad (15)$$

The two unidimensional Hamiltonians are therefore:

$$E = 2p_\eta^2 + \frac{h_z^2}{2\eta^2} + \frac{A\eta}{2} - \frac{\beta + k}{\eta}, \quad (16)$$

$$E = 2p_\xi^2 + \frac{h_z^2}{2\xi^2} - \frac{A\xi}{2} + \frac{\beta - k}{\xi}. \quad (17)$$

The choice of vertical direction for the coordinate frame along the direction of acceleration implicitly imply that  $A$  is positive. Close examination of (16) and (17) shows that it is (16) that has a potential function (last three terms on the right hand side) that has a minimum regardless of any constants because of the positive linear term associated with  $A$ . When motion is possible, orbits are bounded. Motion is possible only if  $E$  is larger than the potential function minimum corresponding to a value that we shall call  $\eta_s$ . The motion in the  $\eta p_\eta$ -plane is shown in Figure (5).

Motion in the  $\xi p_\xi$ -plane depends on the constants of motion as the negative linear acceleration term needs to be compared to the other potential terms that appear in the potential function:

$$W_\xi = \frac{h_z^2}{2\xi^2} - \frac{A\xi}{2} + \frac{\beta - k}{\xi}. \quad (18)$$



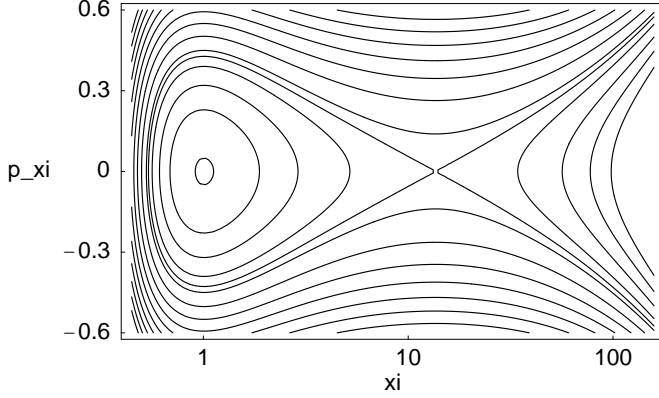


**Fig. 6** Contour plots of the Hamiltonian (17) in the  $\xi p_\xi$ -plane with the parameters  $h_z = 1$ ,  $A = 0.1$ ,  $\beta = 1$  and  $k = 2$ . The separatrix passing through the unstable point at  $\xi_u$  divides space into bounded and unbounded motion.

The derivative of  $W_\xi$  shows that the extrema satisfy the polynomial equation:

$$A\xi^3 + 2(\beta - k)\xi + 2h_z^2 = 0. \quad (19)$$

For  $\beta \geq k$ , this equation has no solution (as  $A$  is positive) and  $W_\xi$  is a monotonic decreasing function. Consequently, motion is unbounded. For  $\beta < k$ , there are extremum points only if:

$$h_z^2 < \left[ \frac{3}{2}(k - \beta) \right]^{\frac{3}{2}} A^{-\frac{1}{2}}. \quad (20)$$

In this case  $W$  has a relative (stable) minimum and a relative (unstable) maximum that we call  $\xi_s$ , and  $\xi_u$  respectively. Bounded motion occurs for  $W_\xi(\xi_s) \leq E < W_\xi(\xi_u)$ ; otherwise orbits are unbounded. Motion in the  $\xi p_\xi$ -plane is shown in Figure (6). The level curves of  $W_\xi$  bear a strong resemblance to the zero-velocity curves of the AKP in cylindrical coordinates (Fig. 2). Whereas the latter curves represent motion boundaries for a given  $h_z$  and  $E$ , the former correspond to actual trajectories. Lastly, we note that the equilibrium orbits derived in section 3, correspond to  $(\xi_s, \eta_s)$  (stable, sombrero profile) and  $(\xi_u, \eta_s)$  (unstable).

## 5 Secular resonance

The physical setting of the AKP is useful in identifying the dynamical response of a planet embedded in a accretion disk that sustains an asymmetric jet system. Such planets form inside the gas disk on circular planar orbits. As the disk's state of least energy is the sombrero profile (Paper II), the formed planet may assume one of the circular sombrero orbits and is therefore immune to any additional dynamical excitation from the acceleration

of the star-disk system. In order to account for the large eccentricity of extrasolar planets through the AKP, the “initial” planetary orbital plane must be inclined with respect the direction of acceleration in order to display the librations described by the two Hamiltonians (Eqn. 16 and 17). The possible physical realization of this geometry is when the jet system is inclined with respect to the star’s rotation axis and therefore precesses around it. In this case, the acceleration has a constant vertical component that defines the sombrero profile and a precessing component that may excite the eccentricity of a planet embedded in the disk. This was the premise of Paper I where the excitation of eccentricity and inclination of extrasolar planets that formed in a jet-sustaining disk was examined.

To illustrate the eccentricity excitation of a planet on an initially circular planar orbit, it is instructive to first consider the situation where the precession frequency is so small that the acceleration appears to maintain a constant inclination with respect to the planetary orbit. In the context of the AKP, studying the excitation due to an inclined constant direction acceleration amounts to choosing initially inclined circular planetary orbits in the presence of a vertical acceleration.

To examine this situation, the AKP was viewed in Paper I as a classical two-body Kepler problem perturbed by the acceleration  $\mathbf{A}$ . Working in the secular regime where the excitation time  $|\mathbf{v}|/A$  is much larger than the orbital period  $2\pi/n$ , the acceleration potential  $R = \mathbf{A} \cdot \mathbf{x}$  was averaged over the orbital period to find:

$$\langle R \rangle = -\frac{3}{2}a \mathbf{A} \cdot \mathbf{e} = -\frac{3}{2}Aae \sin(\varpi - \Omega) \sin I \quad (21)$$

where  $e$  and  $a$  are the orbital eccentricity and semi-major axis. The last expression is obtained by choosing the  $z$ -axis along  $\mathbf{A}$ ; in this case,  $\varpi$ ,  $\Omega$  and  $I$  are the longitude of pericenter, the longitude of ascending node and the inclination of the angular momentum vector  $\mathbf{h}$  with respect to the acceleration  $\mathbf{A}$ . The disappearance of the longitude in the perturbing potential implies that the semi-major axis is constant throughout the evolution.

In terms of orbital elements, the conservation of  $h_z$  can be written as  $\sqrt{1-e^2} \cos I = \cos I_0$ , where  $I_0$  is the initial inclination of the circular orbit. This allows us to reduce the problem to a single degree of freedom with the equations:

$$\dot{e} = -\frac{\sqrt{1-e^2}}{na^2e} \frac{\partial \langle R \rangle}{\partial \omega}, \quad \dot{\omega} = \frac{\sqrt{1-e^2}}{na^2e} \frac{\partial \langle R \rangle}{\partial e}, \quad (22)$$

where  $\omega = \varpi - \Omega$  is the argument of pericenter and  $n = \sqrt{k/a^3}$  is the mean motion. The secular potential is now given as:

$$\langle R \rangle = -\frac{3}{2}Aa \sqrt{\frac{\sin^2 I_0 - e^2}{1-e^2}} e \sin \omega. \quad (23)$$

The orbital elements  $e$  and  $\omega$  therefore follow curves of constant  $\langle R \rangle$ . In particular, the potential  $\langle R \rangle$  (23) has extremum points at:

$$\omega = \pm 90^\circ, \quad e = \sqrt{2} \sin(I_0/2), \quad \text{and} \quad I = \cos^{-1}(\sqrt{\cos I_0}). \quad (24)$$

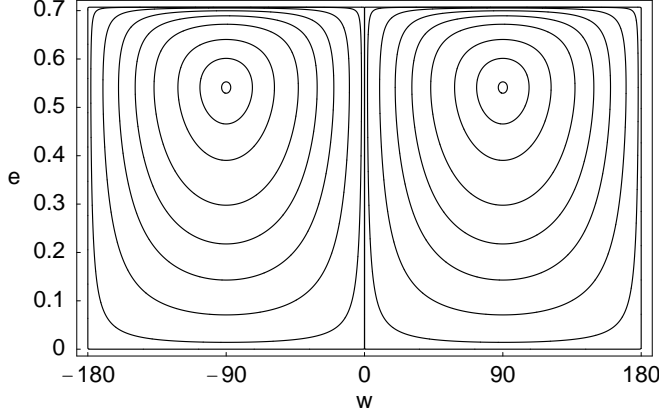


**Fig. 7** Contour plots of the averaged acceleration potential  $\langle R \rangle$  (23) for an initial inclination  $I_0 = 45^\circ$ .

This equilibrium may be interpreted as a secular resonance where the precession rates of the pericenter and node become equal. The maximum value of  $e$  is  $\sin I_0$  and corresponds to the cycle of initially circular orbits. The curves of constant  $\langle R \rangle$  are shown in Figure (7) for an initial inclination of  $I_0 = 45^\circ$ .

The value of  $\langle R \rangle$  being constant throughout the evolution, it is possible to derive the analytical expression of the eccentricity evolution. Denoting by  $C$  the value of  $-2\langle R \rangle / 3Aa$ , the equations (22) yield after some algebra:

$$e^2(t) = \left[ \left( \frac{\sin^2 I_0 + C^2}{2} \right)^2 - C^2 \right]^{\frac{1}{2}} \cos \left[ \frac{3A}{na} t + \phi \right] + \frac{\sin^2 I_0 + C^2}{2}, \quad (25)$$

where  $\phi$  is a phase corresponding to the initial value of  $e$ . The expression of  $\sin \omega$  as a function of time can be deduced from the secular potential (23). For initially circular orbits,  $C = 0$  and  $\omega = 0$  modulo  $180^\circ$ . In this case, equation (25) reduces to the expression given by Equation (8) of Paper I:

$$e(t) = \left| \sin \left[ \frac{3A}{2na} t \right] \sin I_0 \right|. \quad (26)$$

Equation (25) shows that the eccentricity time evolution occurs at the excitation frequency:

$$n_A = \frac{3A}{na}, \quad (27)$$

and that all libration cycles around exact secular resonance possess this same frequency. This was shown to be the case in Paper I where orbits were integrated numerically with the full equations of motion (i.e. without averaging) and a good match was found between the numerical evolution and equation (26) for initially circular orbits.

To understand the origin of the secular resonance in terms of parabolic coordinates, we numerically integrated the equations of motion (3) for orbits

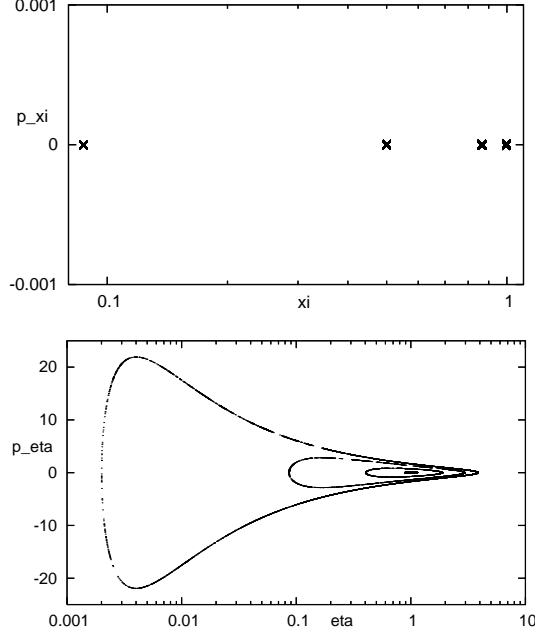


**Fig. 8** Resonance orbits in parabolic coordinate phase space. The AKP parameters are those of a test particle orbiting a solar mass star accelerated by  $A = 5 \times 10^{-11} \text{ km s}^{-2}$ . All orbits share the same initial osculating semi-major axis  $a = 1 \text{ AU}$ , argument of pericenter  $\omega = 90^\circ$ , longitude of ascending node  $\Omega = 0$  and true longitude  $\theta = 0$ . The different orbits correspond to different initial inclinations:  $I_0 = 5^\circ, 30^\circ, 60^\circ$  and  $85^\circ$ ; their eccentricities are given by the expressions (24). The equilibrium position along  $\xi$ -axis is larger for smaller  $I_0$  while the larger  $I_0$ , the larger the  $p_\eta$ -amplitude. The units are AU for  $\xi$  and  $\eta$ , and  $\text{AU year}^{-1}$  for  $p_\xi$  and  $p_\eta$ .

that were initially placed at exact resonance as defined by the osculating orbital elements given by (24). The result is shown in Figure (8). It turns out that exact resonance orbits are on the stable equilibrium  $\xi_s$  in the  $\xi p_\xi$ -plane whereas the corresponding  $\eta p_\eta$ -motion has a finite libration amplitude. This correspondence allows us to derive a geometric property of secular resonance orbits. As  $\dot{\xi} = 0$ ,  $r + z$  (Eqn. 12) is constant for resonant orbits. This in turn shows that resonant motion is confined to the surface of the parabolic paraboloid:

$$z = \frac{\xi_0^2 - \rho^2}{2\xi_0}, \quad (28)$$

where  $\xi_0$  is the initial value of  $\xi$ .

## 6 Keplerian boundary of initially circular orbits

The notion of a boundary in the AKP results from the possible equality at some relative distance of the two bodies of the gravitational interaction and the perturbing acceleration. Unlike the scale invariant classical two-body Kepler problem, the dimension of  $A$  naturally gives rise to a typical length that is proportional to  $(k/A)^{1/2}$ . In Paper I, it was recognized that this length scale had to be an upper bound of the region of bounded motion and that a more precise estimate of the boundary is given by the equality of the mean motion  $n$  and the excitation frequency  $n_A$ . This equality yields the limit beyond which the averaging procedure used in the derivation of  $\langle R \rangle$  (Eqn. 21) breaks down. The corresponding radius is given as:

$$a_{\text{kplr}} = \left[ \frac{k}{3A} \right]^{\frac{1}{2}} \simeq 10^3 \left[ \frac{2 \times 10^{-12} \text{ km s}^{-2}}{A} \right]^{\frac{1}{2}} \left[ \frac{M}{M_{\odot}} \right]^{\frac{1}{2}} \text{ AU}. \quad (29)$$

In terms of  $a_{\text{kplr}}$ , the orbit that defines the outer edge of the sombrero profile (10) is given as:

$$z_{\text{crit}} = \frac{a_{\text{kplr}}}{3} \quad \text{and} \quad \rho_{\text{crit}} = \frac{2\sqrt{2}}{3} a_{\text{kplr}}. \quad (30)$$

Using the formulation of the AKP in parabolic coordinates, it is possible to solve for the radius of the outer boundary of initially circular orbits whose plane normal is inclined to the direction of acceleration such as the orbits of the previous section and those considered in Paper I. These orbits are circular and planar but do not belong to the sombrero profile (i.e. are not least energy orbits) as they are initially inclined. For bounded motion to be possible, the Hamiltonian (17) must have two equilibria. This in turn implies that (17) has three roots at  $p_{\xi} = 0$  for a given initially circular but inclined orbit. These roots are the solution of the equation:

$$E = \frac{h_z^2}{2\xi^2} - \frac{A\xi}{2} + \frac{\beta - k}{\xi}. \quad (31)$$

Calling  $a$  and  $I_0$  the initial osculating semi-major axis and inclination of the circular orbit and taking  $k = 1$ , the constants that appear in (31) are given as:

$$E = -\frac{1}{2a}, \quad h_z^2 = a \cos I_0, \quad A = \frac{1}{3a_{\text{kplr}}^2}, \quad \text{and} \quad \beta = \frac{1}{6} \left( \frac{a}{a_{\text{kplr}}} \right)^2. \quad (32)$$

By substituting these constants into (31) and writing  $\alpha = (a/a_{\text{kplr}})^2/6$  and  $\xi = \Xi a_{\text{kplr}}$ , the three roots may be obtained from the cubic equation:

$$\alpha \Xi^3 - \frac{\Xi^2}{2} + (1 - \alpha)\Xi - \frac{\cos^2 I_0}{2} = 0. \quad (33)$$

The radius of the stable boundary is derived from (33) as the value of  $\alpha$  for which the discriminant of the cubic equation vanishes; in this case, the equation does not admit three distinct real roots. This condition reads:

$$\alpha^4 - 3\alpha^3 + (49 - 18\cos^2 I_0 - 27\cos^4 I_0) \frac{\alpha^2}{16} - \frac{9\alpha\sin^2 I_0}{8} + \frac{\sin^2 I_0}{16} = 0. \quad (34)$$

The solution of the quartic equation can be obtained by the usual standard methods; however, the expressions of the roots are quite cumbersome and are not given here explicitly. Instead, we use the solution of Eqn. (34) directly to plot in Figure (9) the size of the stable boundary,  $a$ , normalized to  $a_{\text{kplr}}$ , (or equivalently  $\alpha$ ) as a function of the initial inclination  $I_0$ . The region of bounded motion occurs inside  $0.72 a_{\text{kplr}}$  for all inclinations and its boundary decreases with increasing inclination,  $I_0$ .

In Paper I, two examples of escape orbits were given: first, for  $a_{\text{kplr}} = 100$  AU an orbit was initially placed at  $a_0 = 68.5$  AU with an inclination of  $I_0 = 30^\circ$  (Figures 7 and 8 of Paper I). At such an inclination, Figure (9) yields a boundary radius of  $a_0 = 68.5$  AU. The chosen orbit was therefore on the unstable equilibrium point of the  $\xi$ -Hamiltonian. The second example was that of the stellar binary companion to  $\nu$  Andromedae. To illustrate how to reach the current orbital configuration of this multiplanet binary system, a time dependent acceleration with a minimum  $a_{\text{kplr}} = 300$  AU was applied to the configuration where the stellar companion was initially placed at  $a = 298$  AU with  $I_0 = 60^\circ$ . In this case, Figure (9) shows that the minimum stable boundary radius corresponds to  $a = 198$  AU. As the acceleration pulse was reaching its maximum, the stable boundary radius decreased from infinity and approached 198 AU. The stellar companion was therefore no longer gravitationally bound to  $\nu$  Andromedae and moved away from it (Figure 14 of Paper I). However as the orbital time of the companion's motion,  $\sim 5000$  years, was larger than the acceleration decay timescale of 2000 years, the stellar companion was not left with enough time to escape before the boundary radius bounced back to infinity. The net result of the acceleration led to the radial migration as well as the eccentricity and inclination excitation of the stellar companion.

## 7 Further developments

In this paper, we have examined the dynamics of the accelerated Kepler problem in detail using the problem's integrability. We have (i) compared the AKP to the classical Kepler problem, (ii) derived analytically the features of least energy orbits, (iii) derived the general solution of the secular problem and interpreted the secular resonance in terms of parabolic variables. Lastly (iv), we used the formulation of parabolic variables to determine analytically the boundary of initially inclined circular orbits that are of particular importance to the problem of radial migration in binary systems as well as to the truncation of accretion disks through stellar jet acceleration.

The AKP's integrability makes it an interesting Hamiltonian system that can be perturbed by additional processes. The perturbation may result in the

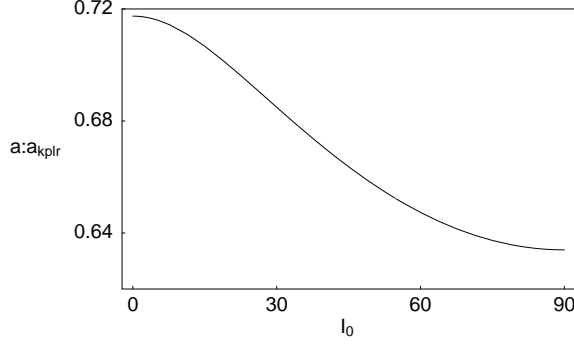


**Fig. 9** The size of the Keplerian boundary of initially circular and inclined orbits in the AKP. The ratio of  $a$  to  $a_{\text{kplr}}$  is shown as a function of  $I_0$  (degrees).

loss of integrability and may lead to possible diffusion. In turn, such mechanisms may further enhance eccentricity excitation and radial migration. In the context of the dynamics of forming protoplanets in a jet-sustaining disk, the modeling of a general time dependence of the perturbing acceleration provides a more realistic model of jet-disk interaction with further consequences such as disk heating (simple examples are given in Papers I and II).

An interesting simple dynamical problem that currently remains unsolved is the possible integrability or quasi-integrability of the precessing AKP. The resonance studied in section 5 illustrated how to excite the eccentricity of an initially circular orbit in the case where the constant-amplitude acceleration has a small precession frequency compared to the excitation frequency  $n_A$ . The more general case of a precessing constant-amplitude acceleration (that corresponds to a precessing jet) yields the precessing AKP equations:

$$\frac{d\mathbf{v}}{dt} = -\frac{k}{|\mathbf{x}|^3} \mathbf{x} + A \mathbf{u}, \quad \text{and} \quad \frac{d\mathbf{u}}{dt} = \boldsymbol{\Omega}_A \times \mathbf{u}, \quad (35)$$

where  $\boldsymbol{\Omega}_A$  denotes the acceleration's constant rotation vector,  $A$  is constant and  $\mathbf{u}$  is the precessing direction of acceleration. To recover the setting of the AKP, two rotations may be applied to (35). First, a rotation at the rate  $\Omega_A$  around  $\boldsymbol{\Omega}_A$  rewrites the equations in the rotating frame where the  $z$ -axis is chosen along  $\boldsymbol{\Omega}_A$ . In this rotating frame, the acceleration (or the vector  $\mathbf{u}$ ) is confined to the  $xz$ -plane and makes an angle  $\alpha$  with the  $z$ -axis. Second, a rotation of angle  $\alpha$  around the  $y$ -axis makes the direction of acceleration along  $z$ . The corresponding transformations are simple to carry out and the resulting equations are:

$$\ddot{X} - 2\Omega_A \cos \alpha \dot{Y} = \Omega_A^2 (\cos^2 \alpha X + \sin \alpha \cos \alpha Z) - \frac{kX}{(X^2 + Y^2 + Z^2)^{3/2}}, \quad (36)$$

$$\ddot{Y} + 2\Omega_A (\cos \alpha \dot{X} + \sin \alpha \dot{Z}) = \Omega_A^2 Y - \frac{kY}{(X^2 + Y^2 + Z^2)^{3/2}}, \quad (37)$$

$$\ddot{Z} - 2\Omega_A \sin \alpha \dot{Y} = \Omega_A^2 (\sin \alpha \cos \alpha X + \sin^2 \alpha Z) - \frac{kZ}{(X^2 + Y^2 + Z^2)^{3/2}} + A. \quad (38)$$

With respect to the AKP, precession introduces the Coriolis force (second term on the left hand side of each equation) and the centrifugal force with respect to the rotation vector  $\Omega_A$  (first term on the right hand side of each equation). The momenta of the precessing AKP are given as:

$$p_X = \dot{X} - \Omega_A Y \cos \alpha, \quad (39)$$

$$p_Y = \dot{Y} + \Omega_A (X \cos \alpha + Z \sin \alpha), \quad (40)$$

$$p_Z = \dot{Z} - \Omega_A Y \sin \alpha, \quad (41)$$

and the corresponding Hamiltonian is:

$$H = \frac{p^2}{2} + \Omega_A Y (p_X \cos \alpha + p_Z \sin \alpha) - \Omega_A p_Y (X \cos \alpha + Z \sin \alpha) - \frac{k}{|\mathbf{X}|} - AZ. \quad (42)$$

This in turn shows that the energy integral of the AKP is:

$$E = \frac{\dot{X}^2 + \dot{Y}^2 + \dot{Z}^2}{2} - \frac{\Omega_A^2}{2} [(X \cos \alpha + Z \sin \alpha)^2 + Y^2] - \frac{k}{|\mathbf{X}|} - AZ. \quad (43)$$

As axisymmetry has now been lost, the vertical component of angular momentum is not conserved. We have searched for analytic integrals of the precessing AKP without much success. We note however that averaged precessing AKP is integrable and that an exact analytical solution was derived in Paper I. Further numerical investigations will shed some light on the integrability of the precessing AKP.

## References

1. B.H. Bransden and C.J. Joachain, Introduction to Quantum Mechanics. Addison Wesley Longman Limited. (1989)
2. P.S. Epstein, Zur Theorie des Starkeffektes, Annalen der Physik **50**, 489 (1916)
3. L.D. Landau and E. M. Lifshitz, Course of Theoretical Physics. Pergamon Press Oxford. (1969)
4. F. Namouni, On the origin of the eccentricities of extrasolar planets, AJ **130**, 280 (2005) (Paper I)
5. F. Namouni, J.L. Zhou, The influence of mutual perturbations on the eccentricity excitation by jet acceleration in extrasolar planetary systems. CMDA **95**, 245 (2006)
6. F. Namouni, On the flaring of jet-sustaining accretion disks. ApJ **659**, 1510 (2007) (Paper II)
7. P.J. Redmond, Generalization of the Runge-Lenz Vector in the presence of an electric field, Physical Review **133**, B1352 (1964)
8. A. Sommerfeld, Atombau und Spektrallinien. Braunschweig: Vieweg & Sohn. (1929)